IEEE Access
Multidisciplinary | Rapid Review | Open Access Journal

Received August 21, 2019, accepted August 28, 2019, date of publication August 30, 2019, date of current version September 13, 2019.

Digital Object Identifier 10.1109/ACCESS.2019.2938454

Space Target Detection in Complicated Situations for Wide-Field Surveillance

MENGYANG LI[1,2], CHANGXIANG YAN[1,3], CHUNHUI HU[1], CHONGYANG LIU[1,2], AND LIZHI XU[1,2]

[1]Changchun Institute of Optics, Fine Mechanics and Physics, Chinese Academy of Sciences, Changchun 130033, China
[2]University of Chinese Academy of Sciences, Beijing 100049, China
[3]Center of Materials Science and Opto-Electronics Engineering, University of Chinese Academy of Sciences, Beijing 100049, China

Corresponding author: Changxiang Yan (yancx0128@126.com)

This work was supported in part by the National Key Research and Development Program of China under Grant 2016YFF0103603, in part by the Technology Development Program of Jilin Province, China, under Grant 20180201012GX, and in part by the National Natural Science Foundation of China under Grant 61627819, Grant 61805235, and Grant 61875192.

ABSTRACT Long exposure time and wide field can effectively improve the ability of a space surveillance telescope to detect faint space targets. However, complicated situations pose challenges for space target detection. Background star images usually manifest a rotated streak, and target trajectories can be crossed, discontinuous, or nonlinear. This paper presents an accurate and robust space target detection method, namely, spatiotemporal pipeline multistage hypothesis testing (SPMHT), to overcome the issues. Specifically, the method includes the following two stages: First, in the spatiotemporal pipeline filtering step, Spatiotemporal-related Intersection over Union (SrIoU) is used to calculate the IoU score instead of the traditional method. Benefiting from the differences between motion characteristics of targets and stars and the insensitivity of the SrIoU score to the noise, the spatiotemporal pipeline filtering can effectively remove the streak images of background stars and obtain candidate points. Second, a series of candidate points is further organized into a tree structure. We pruned in the tree structure combined with these candidate trajectories by using velocity and direction feature of moving objects. Furthermore, in the search step, fast adaptive sequence region search is used to reduce the computational cost. The experimental results for two datasets, simulated image datasets and real captured image datasets, demonstrate the effectiveness in addressing the difficulties of space target detection in complicated situations.

INDEX TERMS Space target detection, wide-field surveillance, complicated situations, spatiotemporal pipeline, multistage hypothesis testing (MHT).

I. INTRODUCTION

Space targets, including nonfunctional artificial objects, spent upper stages, and apogee boost motors, are mainly satellites and space debris of all sizes in near-earth space. With the development of human space activities, the number of space targets has rapidly increased [1], [2]. If such a large number of space targets collide with one other, then this will become a remarkable threat to human space activities [3]. Therefore, space target detection for wide-field surveillance is vital in predicting and avoiding these types of threats.

Space targets appear to be small point-like or streak-like sources with low intensity, faintly reflecting the light from stars in a single frame image [4]–[6]. When a charge-coupled device (CCD) image sensor focuses on the same region in space, the pieces of space targets imaged on the focal plane of these sensors only cover a small number of pixels. Therefore, feature-based methods, such as scale invariant feature transform (SIFT) [7], local binary pattern (LBP) [8], and histogram of oriented gradient (HOG) [9], fail to detect faint and small space targets in a single frame image. Many algorithms for detecting faint and small targets from images with low SNR or strong interferences have been proposed, especially for applications in infrared surveillance [10]–[12], small target measurement and tracking [13]–[19]. Frame-by-frame differencing and thresholding operations [20] have traditionally been used for this purpose. However, the small size and slow motion of space targets in the image sequence pose remarkable difficulties in the effectiveness of the algorithm. Reed *et al.* [21] developed a robust approach for detecting

The associate editor coordinating the review of this article and approving it for publication was Habib Ullah.

This work is licensed under a Creative Commons Attribution 4.0 License. For more information, see http://creativecommons.org/licenses/by/4.0/

weak moving targets by using three-dimensional (3-D) matched filtering. Their method performs matched filtering for moving target signatures in the Fourier domain with proper signal phasing automatically applied to sum the target energy and reduce background noise. However, pairing the matched filter to a specific velocity profile, which is a known target moving at a known speed in a designated direction, is the disadvantage 3-D matched filtering. A series of algorithms, such as the stacking method [22] and line-identifying technique, was proposed to solve this problem. Mohanty [23] demonstrated that potential track trajectories of a weak point target can be assembled through a comprehensive search of all possible trajectories in a given frame sequence that outputs results based on the maximum likelihood ratio. Barniv [24] proposed a method that uses specific knowledge of potential speed windows and target shapes to attempt to reduce the large computational cost in searching trajectories. Cowart *et al.* [25] used a Hough transform for detecting streaks in images. Fujita *et al.* [26] used a technique called the improved optical flow algorithm to estimate motion vectors of objects in an image sequence and subsequently detect unknown space target trajectories. Fujita *et al.* [27] developed a novel method to detect trajectories by using numerical evaluation on the direction of line segments and continuity of the image objects in a line segment. These methods are effective in detecting faint and small space targets in image sequences. However, these algorithms are limited by the large computational cost that comes with the large number of possible trajectories that must be searched. Furthermore, these techniques only detect continuous and linear trajectories in the image sequence and are unsuitable for discontinuous and nonlinear ones.

Blostein and Huang [28] proposed an efficient algorithm called multistage hypothesis testing (MHT) for the detection of faint and small moving objects with unknown position and velocity in an image sequence. The background image pixels can be modeled as Gaussian random variables. A large number of objects in an image sequence are organized into a dense set of space-time candidate trajectory segments. A tree structure combined with these candidate trajectories is established and then pruned at every pixel in every image of the sequence by using hypothesis testing. Finally, the objects whose trajectories are consistent with all the hypothesis testing stages are considered true objects. On this basis, many improved algorithms, such as SB–MHT [29], MMHTT [30], and TMQHT [31], have been proposed subsequently. Although these methods are effective in detecting and tracking faint small objects in the star background, the following difficulties and challenges still exist. First, the computational cost is still large because detection is performed at every pixel in every image of the sequence. Second, in MHT experiments, at least 10 test stages are required for object detection to reduce the number of false alarms. Therefore, 10 images should be stored until the detection process is completed, and the candidate trajectories increase rapidly as the number of test stages increases. The number of image sequences can still be reduced if the prior information of moving objects can be used during detection. Third, background star images usually manifest a rotated streak, and target trajectories can be crossed, discontinuous, or nonlinear in long exposure time and wide-field space surveillance of the telescope. Consequently, complicated situations will pose difficulties and challenges for space target detection.

To solve these problems, we propose a high-accuracy and robust two-stage object detection framework named Spatiotemporal Pipeline Multistage Hypothesis Testing (SPMHT) while maintaining a low computational cost. Through three efforts, we improve the detection accuracy and robustness in complicated situations. First, considering that the targets with different orbital altitudes have different velocity and direction of motion, the inter-frame motion of the target is modeled. We use angle-related Anisotropic Gaussian Spread Function to obtain the center coordinate and angle parameters of the streak-like target. The inter-frame motion distance of the targets can be further calculated as the basis for choosing the adaptive search range in the stage of multistage hypothesis testing. Second, the background stars and noise are removed by using the proposed modified spatiotemporal pipeline filtering method. We establish a circular region on the centroid of targets rather than at every pixel in every sequence image, and only the pixels in the spatiotemporal pipeline are processed, which can overcome the influence of streak images of background stars and reduce the large computational cost. The SrIoU score is used to target classification in the spatiotemporal pipeline filtering instead of the traditional gray-value correlation method. Benefiting from the differences between motion characteristics of targets and stars and the insensitivity of the SrIoU score to the noise, the detection probability of low SNR targets is improved. Third, hypothesis testing is carefully designed, thus, the targets with various velocity and direction can match a sufficient number of candidate points to ensure the detection probability for nonlinear and discontinuous trajectories. The Fig. 1 shows the block diagram of the proposed method.

This paper is organized as follows: Section 2 analyzes the features of background stars and space targets in single frame and sequence images, respectively. Section 3 describes the proposed SPMHT method. Section 4 presents the simulation and experimental results. Finally, Section 5 summarizes the conclusions of the study.

II. IMAGING CHARACTERISTICS

The optical image is modeled as follows

$$F(i,j,k) = T(i,j,k) + S(i,j,k) + B(i,j,k) + N(i,j,k) \quad (1)$$

where k is the frame index of the image sequence, and $F(i,j,k)$ represents the grayscale value at the integer space coordinate (i,j) in the k-th frame of the image sequence. $T(i,j,k)$ and $S(i,j,k)$ denote the space targets and stars, respectively, wherein both can be modeled with a

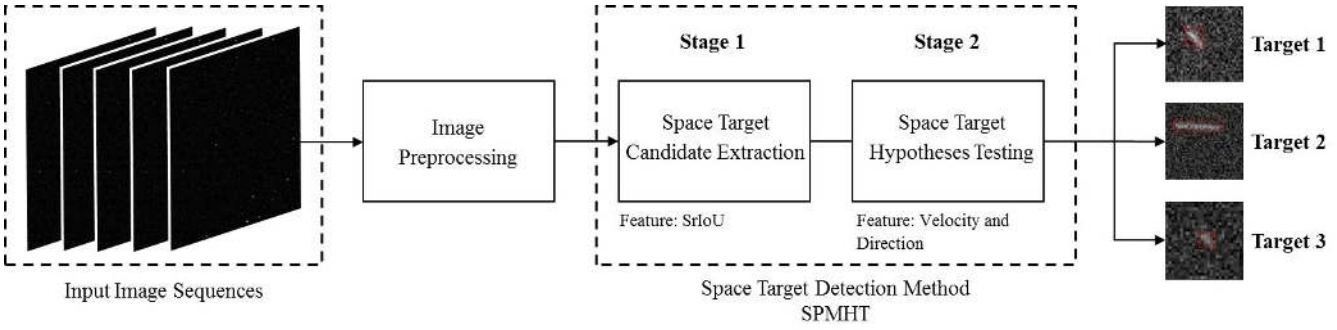

FIGURE 1. Workflow of our proposed method.

Gaussian profile. $B(i, j, k)$ refers to the background, which is often nonuniform because of the effects of stray light and the signals from different CCD channels. The noise $N(i, j, k)$ is generated by the hot pixels at fixed positions of the images due to space radiation, flicker noise at random positions of images coming from space radiation, a combination of several kinds of noises, and the dark current.

In this section, we analyze the features of background stars and space targets in single frame and sequence images, respectively. Research on imaging characteristics is crucial to the performance of detection algorithms.

A. CHARACTERISTICS OF OBJECT IN SINGLE FRAME

In the sidereal tracking mode, an ideal star (without platform vibration in a short exposure time) appears to be a point-like source with the center at the maximum of the two-dimensional (2-D) Gaussian function. The point spread function (PSF) is defined by the Gaussian function. However, the platform vibration and tracking error in a long exposure time in single frame cause the background stars to appear short and streak-like. In this situation, the horizontal spread radius is not equal to the vertical spread radius ($\sigma_x \neq \sigma_y$). Moreover, the space target is streak-like source in random direction. The traditional Gauss model is difficult to represent these characteristics. To solve this problem, we applied the angle-related Anisotropic Gaussian Spread Function to construct a streak-like object imaging model.

$$f(x, y) = A \cdot \exp\left\{ -\frac{[(x - x_0)\cos\theta + \left(y^{'} - y_0\right)\sin\theta]^2}{2\sigma_x^2} - \frac{[(x - x_0)\sin\theta - (y - y_0)\cos\theta]^2}{2\sigma_y^2} \right\} \quad (2)$$

where A, σ_x, and σ_y refer to the maximal energy, horizontal spread radius, and vertical spread radius of the object, respectively. The orientation parameter, θ, determining the rotation angle of the object, is defined as the angle between original coordinate system and new coordinate system from 0 to π, as shown in Fig. 2. The coordinates (x_0, y_0) and (x, y) describe the object center and the positions of the distributed pixels, respectively.

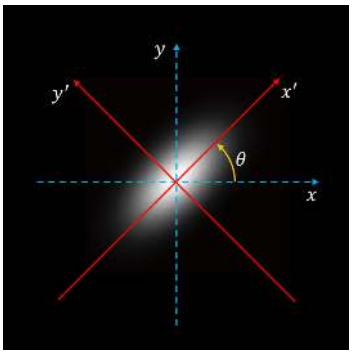

FIGURE 2. Angle-related imaging model.

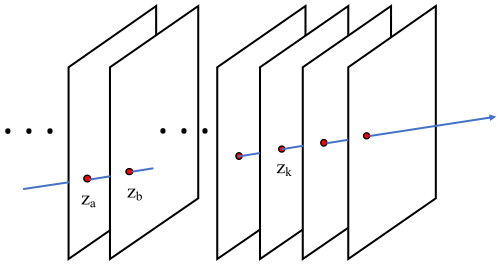

FIGURE 3. Trajectory model of the space target in the sequence images.

B. CHARACTERISTICS OF OBJECT IN SEQUENCE IMAGES

In the sequence images, the trajectory of the space target is an ordered set of mutually similar primitives with regular locations in the spatiotemporal distribution and consistent speed in the primitive shape.

Therefore, we are modeling a single track. A line in the spatiotemporal location is given to correspond to a thought trajectory of object. If we obtain Z_a and Z_b, which are the locations of two key primitives representing the line, then the spatiotemporal location Z_k will be obtained by the following equation:

$$z_k = z_a + (k - k_a)\frac{z_b - z_a}{k_b - k_a}, \quad k = 1, 2, ..., n \quad (3)$$

where k is the frame index of the image sequence, and k_a and k_b are their indices (See Fig. 3).

In the inter-frame, space target make an apparent motion during the long exposure time. At time t, the primitive

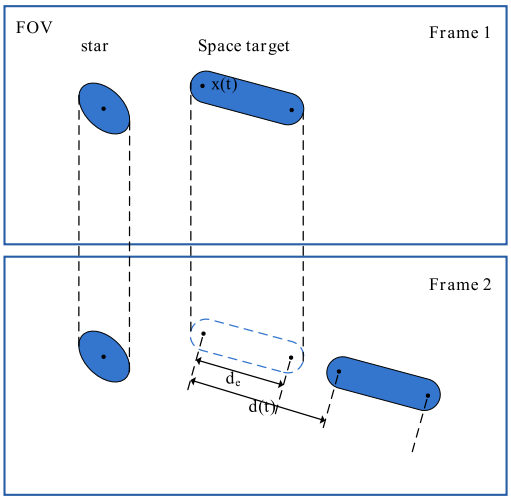

FIGURE 4. Motion model for space target and star in the inter-frame during long exposure time.

position of space target is $x\,(t)$. During the exposure time, its streak length is d_e, which can be approximated by the length of the major axis of the connected component. The next time this space target is observed, it has moved to $x\,(t+\Delta t)$, where the observational interval is $\Delta t = t_e + t_r$, in which t_e is the exposure time (3 s in our data), and t_r is the readout plus the wait time (See Fig. 4). The relative inter-frame motion vector $d\,(t)$ can be used as the basis for choosing the adaptive search range in the stage of multistage hypothesis testing. $d\,(t)$ is then obtained as follows:

$$d\,(t) = x\,(t + t_e + t_r) - x\,(t) = \frac{\Delta t}{t_e} d_e \tag{4}$$

III. SPACE TARGET DETECTION

A. PREPROCESSING OF SEQUENCE IMAGES

In this work, the sequence images are preprocessed for efficient application to the proposed methods, which will be described in the following subsections. The steps of the preprocessing method are described as follows:

Step 1: Median filtering is selected to remove the discrete noise. The median-filtered image is obtained by computing the following median value of every pixel in the frame set:

$$g\,(i,j) = median\,[f\,(i-k, j-l)]\,, \quad (k,l \in W) \tag{5}$$

where $f(i,j)$ and $g(i,j)$ denote the original and median-filtered images, respectively, and W represents the median filter mask.

Step 2: For each image frame, the grayscale value threshold of the background is selected to generate the binary image. The formula for the segmentation threshold is presented as follows:

$$b(i,j) = \begin{cases} 1, & g(i,j) > T \\ 0, & g(i,j) \le T \end{cases} \tag{6}$$

where T denotes the grayscale value threshold for binarization, and $b(i,j)$ represents the image after binary segmentation. Threshold T can be calculated by using the average value μ and standard deviation σ in the first three lines of the image data as follows:

$$T = \mu + 2\sigma \tag{7}$$

Step 3: Labeling is conducted for a series of low signal-to-noise ratio (SNR) and streak-like target pixels, which will cause a problem when the same target in the binary image is regarded as the different image region.

Therefore, we applied the ''close'' operation in morphological filtering to eliminate the noise in the image by using a flat disk-shaped structuring element Φ with a specified radius. The binary mask containing the space targets and background stars can then be defined as

$$B(i,j) = b(i,j) \bullet \Phi \tag{8}$$

where $\bullet$ is the ''close'' operation in morphological filtering.

Step 4: For the labeled images in step 3, image regions with isolated pixels (less than 3 pixels) are removed from each image frame.

B. PROPOSED METHOD

In this section, we detail the proposed SPMHT method. First, a spatiotemporal pipeline filtering method is presented to remove the streak images of background stars effectively and obtain candidate points by SrIoU score. Second, a series of candidate points is further organized into a tree structure, hypothesized in moving velocity and direction at each center of the points in the sequence, and tested sequentially whether it constitutes a trajectory. The candidate points whose trajectories are consistent with all the hypothesis testing stages are considered the true space targets.

1) SPATIOTEMPORAL PIPELINE FILTERING AND SrIoU

The traditional pipeline method is to detect the number of times the target appears in the pipeline. It is considered that there are targets in the pipeline if the number of times the target appears is greater than the set threshold. This method is effective in detecting dim and small targets from background (continuous background, which only includes clouds, sky, and sea) in infrared images. However, it is difficult to distinguish the space targets from background stars in star background images.

Inspired by this study, considering the characteristics of the space target and background star, the spatiotemporal pipeline filtering (SPF), which can be effectively applied to target detection in star background images, was designed, as shown in Fig. 5. In the sequence images, we use three parameters, center position, diameter and length, to generate spatiotemporal pipelines and effectively cover the objects of different shapes and SNRs. The center position is determined by the center coordinate of the object in the current frame. The diameter of the pipeline represents the neighborhood size of the object, and the length of the pipeline represents the number of frames needed for detection.

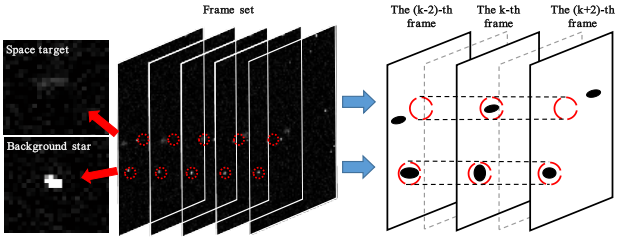

FIGURE 5. Framework diagram of spatiotemporal pipeline filtering.

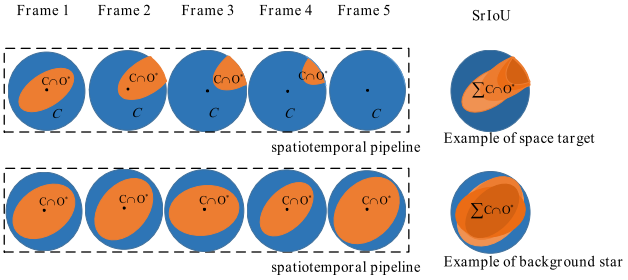

FIGURE 6. Calculation approaches of SrIoU in the spatiotemporal pipeline.

The circular region in each frame shows that the position of the background star barely changes, but the position of the space target is clearly different because of its motion characteristics in the sequence image. The calculation method and the threshold setting of this difference are crucial for the SPF-based detection algorithm. Fujita *et al.* [26] described this difference by BM algorithm. Many functions, such as Normalized Cross Correlation (NCC), Sum of Absolute Difference (SAD), Sum of Squared Difference (SSD), are used to evaluate the degree of coincidence between two block images appropriately selected in the different image frames. When the BM algorithm is applied to the different image frames, one issue is concerned with heavy computational load mainly caused by matching process for the second frame from the same location in the first frame. Another issue is the evaluation score is sensitive to the change in the gray values of pixels, and image noise causes a rapid decrease in the evaluation score. In addition, the detection for blinking targets which discontinuously appears in the sequence images, tends to fail when the image frame does not contain the corresponding targets.

To solve these problems, we applied the spatiotemporal-related IoU (SrIoU) to calculate the IoU between the circular pipeline-region C and the object region O, instead of applying the BM algorithm, as shown in Fig.6. The circular pipeline-region C is defined by the 4-tuple coordinate (x, y, d, k), where (x, y) represents the geometric center coordinate of the circular pipeline-region; d and k are the diameter of the circular pipeline-region and the length of the pipeline, respectively.

In this work, the spatiotemporal pipeline is generated in the binary sequence images. The diameter and length of the pipeline are set to 5 pixels and 5 frames, respectively.

The calculation method of the SrIoU is expressed as follows:

$$SrIoU(\mathrm{C}, \mathrm{O}) = \frac{\sum_1^k area(\mathrm{C} \cap \mathrm{O}^*)}{\sum_1^k area(\mathrm{C} \cup \mathrm{O}^*)} \tag{9}$$

where $C(x_c, y_c, d_c, k_c)$ is the circular pipeline-region with the diameter d_c and the frame index k_c. O is the nearby binary object region and O^* is defined as pixels of the nearby binary object region covered by the circular pipeline-region. K represents the number of frames needed for detection. In our proposed spatiotemporal pipeline method, K is set to 5 to exclude the influence of the blinking background star and improve the detection ability of low SNR targets effectively. Although the number of frames increases in this process, the computational load for the proposed method is low compared with the original correlation-matching algorithm. We can exclude a large number of background stars and obtain candidate points of the space targets in the single image.

The spatiotemporal pipeline filtering method divides the positive and negative objects based on the SrIoU scores, which is defined as (10).

$$\begin{aligned} &\text{positive(space target)} : \text{scores} < t_s \\ &\text{negative(background star)} : \text{scores} > t_s \end{aligned} \tag{10}$$

A loose SrIoU threshold encourages more object regions to be classified into the space targets, which introduces more false positives, whereas, a tight SrIoU threshold substantially reduces the number of positives but introduces lower precision. To solve these problems, SPMHT uses two stage detection method to improve the detection probability. For the first stage, the positive and negative objects are divided by a loose SrIoU threshold ($t_s = 0.6$) to ensure the detection probability. This process focuses only on the extraction of the candidate points, and does not involve the object category determination. In the second stage, the strict hypothesis testing conditions are employed as the criteria for selecting the positive target, and the false alarm targets are further removed. This process is beneficial for improving the detection probability and reducing the computational cost.

2) FAST ADAPTIVE SEQUENCE REGION SEARCH AND MULTISTAGE HYPOTHESIS TESTING

After the removal of background stars, in stage two, we can obtain candidate points in the image sequences. Instead of global search, region search method with fixed radius is proposed in [31], used to reduce the computational load. However, one problem that deserves special attention is that space targets with different orbital altitudes have different velocity and direction of motion. If we simply set the search direction and distance to a fixed value, respectively, we may lose targets with different orbital altitudes.

To address this problem, we introduce a Fast Adaptive Sequence Region Search. A Fast Adaptive Sequence Region Search is first used to determine whether the candidate point

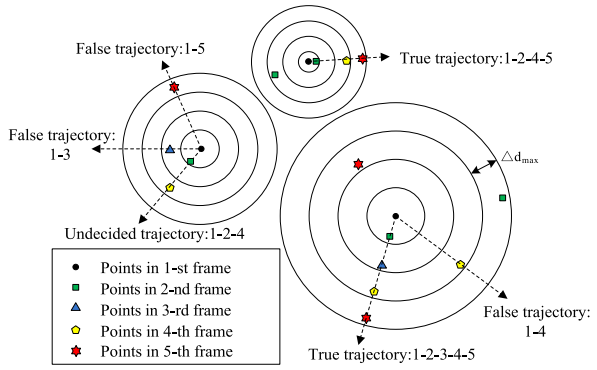

FIGURE 7. Fast adaptive sequence region search of SPMHT.

appears in the next frame. If we know the distance of target motion in a single frame and the time interval of exposure between frames, we can predict the possible location of space target in the next frame. We can obtain candidate point $Z(i, j, k)$ in the space targets, where (i, j) is the coordinates of the center of the candidate points and the frame set number k is set to $1 \leq k \leq 5$. The proposed SPMHT algorithm is initiated with the candidate point $Z(i, j, 1)$ of space targets with frame index 1 as the root nodes to search for the trajectory points with frame indices 2, 3, 4, and 5 of the image sequence. The maximum and minimum inter-frame motion distances of all the space targets are denoted by $d_{\max}$ and $d_{\min}$ in the image sequence, respectively. The value of $d_{\max}$ and $d_{\min}$ are $1.5d(t)$ and $0.5d(t)$, respectively. A search radius between $d_{\min}$ and $d_{\max}$ centered on initial point Z_a is created, and point Z_b and initial vector $\overrightarrow{z_a z_b}$ are obtained. The maximum search radius for each frame index is $d_{\max}$, $2d_{\max}$, $3d_{\max}$, and $4d_{\max}$. Meanwhile, the minimum search radius ($d_{\min}$, $2d_{\min}$, $3d_{\min}$, $4d_{\min}$) for each frame index should be satisfied. The Fig. 7 shows that candidate points are then selected to determine whether hypothesis testing conditions are satisfied in each frame. A highlight of this method is that it only needs to search for different orbital altitude targets in each frame once in the adaptive region. Therefore, this method significantly saves computational time and detects space targets with different orbital altitudes efficiently.

A series of candidate points is further organized into a tree structure, hypothesized in moving velocity and direction at each center of the points in the sequence, and tested sequentially whether it constitutes a trajectory. Each piece of space target is assumed to have its own constant velocity and fixed moving direction.

Two kinds of hypotheses are defined as

H_1: The candidate point is on the moving trajectory.

H_2: The candidate point is not on the moving trajectory.

The hypothesis testing conditions are given by

$$\begin{cases} \left| \dfrac{|\overrightarrow{z_a z_b}|}{|k_a - k_b|} - \dfrac{|\overrightarrow{z_a z_k}|}{|k - k_b|} \right| \leq d \\ \left| \cos\langle \overrightarrow{z_a z_b}, \overrightarrow{z_a z_k} \rangle - 1 \right| \leq \theta \end{cases} \Rightarrow \text{choose } H_1 \\ \text{otherwise.} \Rightarrow \text{choose } H_2 \tag{11}$$

where Z_a, Z_b, and Z_k are the three points with different frame indices in a frame set. Their centroids are (x_a, y_a), (x_b, y_b), and (x_k, y_k), and their frame indices are denoted by k_a, k_b, and k, respectively. In this study,

$$|\overrightarrow{z_a z_b}| = [(x_b - x_a)^2 + (y_b - y_a)^2]^{1/2} \tag{12}$$

$$|\overrightarrow{z_a z_k}| = [(x_k - x_a)^2 + (y_k - y_a)^2]^{1/2} \tag{13}$$

$$\cos\langle \overrightarrow{z_a z_b}, \overrightarrow{z_a z_k} \rangle = \frac{\overrightarrow{z_a z_b} \cdot \overrightarrow{z_a z_k}}{|\overrightarrow{z_a z_b}|\,|\overrightarrow{z_a z_k}|} \tag{14}$$

The thresholds of the distance and cosine value of degree are denoted by d and θ, respectively. θ can be selected as $\theta \in (0, 0.1)$, but d cannot be set to a fixed value due to the different speeds of space targets with different orbital altitudes. We can obtain the relative inter-frame motion vector $d(t)$ of different space targets by using Eq. (4). Thus, d can be set to $d \in (0.5d(t), 1.5d(t))$.

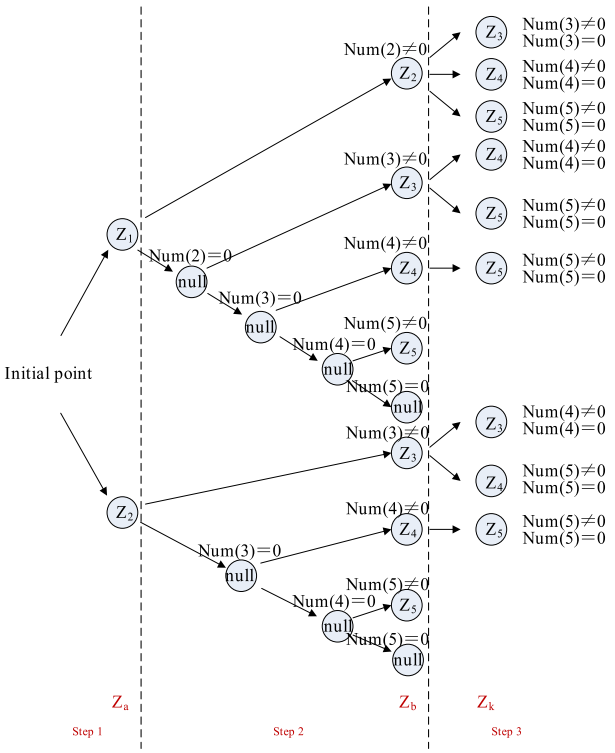

FIGURE 8. Search tree of SPMHT.

We start the search from initial point Z_1 in the single frame index image. However, space targets may lose the first point of the trajectory in the frame set. The search will fail when a target discontinuously appears in the sequence image and no corresponding point exists in the first frame. Therefore, Fig. 8 shows that a technique is proposed to address the issue. We used the points in the second frame that do not satisfy the hypothesis testing conditions as the new initial point Z_2 to start the search. Moreover, unlike the original progressive search by frame, we propose a parallel search tree. The number of hypothesis testing and computational

load will decrease in this process compared with those of the original search method.

The total number of candidate points with frame index k that fall in the search area starting from Z_1 is denoted by Num (2), Num (3), Num (4), and Num (5). Fig. 8 shows that the proposed SPMHT algorithm is subsequently performed based on the search tree.

Step 1: We take point Z_1 and Z_2 in the first and second frames as the initial points of the search, respectively.

Step 2: Our purpose is to find point Z_b, which satisfies the maximum and minimum inter-frame motion distance conditions, to form the initial vector $\overrightarrow{z_a z_b}$ with initial point Z_a. Null indicates that no point in the current frame satisfies the maximum and minimum inter-frame motion distance conditions. In this case, search the next frame until we find point Z_b, which satisfies the hypothesis testing conditions.

Step 3: We determine whether point Z_k in the rest of the frames satisfies the hypothesis testing conditions in Eq. (11).

Each candidate trajectories is then scored. The number of candidate points that satisfies the hypothesis testing conditions is used to determine whether a true space target is in the frame set as follows:

$$\sum_{k=1}^{K} P_k \begin{cases} \geq D_1 & \Rightarrow \text{true trajectory} \\ \leq D_2 & \Rightarrow \text{false trajectory} \\ \in (D_1, D_2) & \Rightarrow \text{undecided trajectory} \end{cases} \tag{15}$$

where P_k is the number of the candidate point that satisfies the hypothesis testing conditions in a frame set, and D_1 and D_2 are decided based on the image number K of the frame set. In this study, given that $K = 5$, $D_1 = 4$ and $D_2 = 2$ are selected.

For undecided points, proceed to next frame set. The tests are performed as follows:

$$\sum_{k=1}^{K_2} P_k \begin{cases} \geq D_3 & \Rightarrow \text{true trajectory} \\ < D_3 & \Rightarrow \text{false trajectory} \end{cases} \tag{16}$$

where $K_2 = 2 \times K = 10$ and $D_3 = 6$.

Finally, the candidate points whose trajectories are consistent with all the hypothesis testing stages are considered the true space targets.

Computational Cost: In the original MHT [28] method, the detection is performed at every pixel in every image. Suppose $K = N_{sets} \times K_0$ frames of images with $M \times N$ pixels exist. Thus, the total number of searches in the MHT method is $(MN)^K$. In the improved method [31], the K frames of images are separated into N_{sets} frame sets, and each set has $K_0 (K_0 > 3)$ images. If the maximum number of candidate points (including space targets and false alarms) among all K images is N_{max}, then $N_{max} < MN$. The maximum total number of searches in the TMQHT method is $N_{sets} N_{max}^{K_0}$. In our proposed SPMHT method, the candidate points are first used to construct candidate vectors, and the points of the rest frames are judged by hypothesis testing in parallel. Thus, the number of searches is $N_{max}^2 (K_0 - 2) N_{max}$, then $K_0 > 3$. The maximum computational cost of the SPMHT method, which performs searches on the candidate points among frame sets, is $N_{sets} N_{max}^2 (K_0 - 2) N_{max}$.

$$N_{sets} N_{max}^2 (K_0 - 2) N_{max} < N_{sets} N_{max}^{K_0} < (MN)^K \tag{17}$$

Thus, the proposed SPMHT method has considerably fewer computational cost than the [28] and [31] method.

IV. EXPERIMENTS AND DISCUSSIONS

In this section, we conduct some experiments to verify the performance of our space target detection method. First, we model and generate background stars and space targets according to the Tycho-2 Catalogue. Then, we run the whole detection framework in different simulated image datasets and real image datasets, respectively. Finally, we conduct a comparative experiment on the capability of our SPMHT algorithm and other state-of-art algorithm. The algorithm is programmed using Matlab and C++. All the experiments were carried out on a computer equipped with Intel Xeon CPU X5690 (8 cores, 3.47 GHz), 96 GB memory, and NVIDIA Quadro 6000.

To quantitatively evaluate the detection performance, we utilized the evaluation indicators of detection probability P_d, false alarm rate P_f, and receiver operating characteristic (ROC) curves as well as area under curve (AUC).

ROC curves have been widely used as a performance evaluation tool in target detection applications [35]. The ROC reflects the detection probability of the detector at different false alarm rates. Detection probability and false alarm rate are calculated from the true positive (TP), false positive (FP), true negative (TN) and false negative (FN). In object detection task, TP represents the number of detected true targets at a certain threshold; FP represents the number of false alarms mistaken as targets; TN represents the number of false alarms correctly classified; FN represents the number of true targets which are not correctly predicted; and GT represents the total number of true targets. Based on these components, detection probability P_d and false alarm rate P_f are defined as follows:

$$P_d = \frac{TP}{TP + FN} = \frac{TP}{GT} \tag{18}$$

$$P_f = \frac{FP}{FP + TN}, \tag{19}$$

The AUC metric is an evaluation metric that combines detection probability and false alarm rate, which reflects the global performance. AUC is the integral of the area under the ROC curves.

A. MODELING AND GENERATION OF BACKGROUND STARS AND SPACE TARGETS

In the extremely small angular dimensions of stars, the single star image irradiance distribution is the PSF of optics. PSF is imaged as a circular spot called "Airy disk."

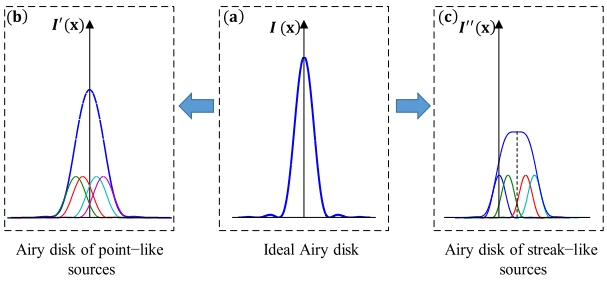

FIGURE 9. 2-D Airy disk model.

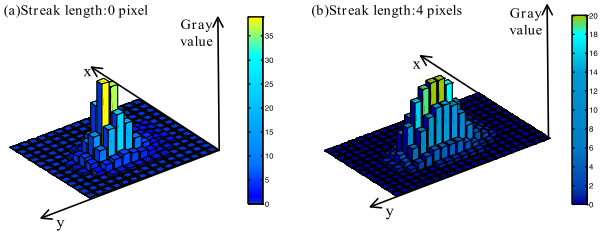

FIGURE 10. 3-D grayscale histogram of the streak-like airy disk model.

The Airy disk model is used to simulate static stars and static space targets [32]. This model is defined as

$$I(\Phi) = \begin{cases} I_0, & \Phi = 0 \\ I_0 \left[\dfrac{2J_1(\Phi)}{\Phi} \right]^2, & \Phi \neq 0 \end{cases} \tag{20}$$

where I_0 is the central intensity of the stars, J_1 is the Bessel function of the first kind, $\Phi = ((x-x_0)^2+(y-y_0)^2)^{1/2}$, where (x_0, y_0) is the central coordinates of the stars, and x and y are the axes starting from the center pixel of the stars in the horizontal and vertical directions, respectively. The stars and space targets located in different positions in the exposure time can be simulated by moving the centroid (x_0, y_0) of the Airy disk. A total of 80% energy is found in a 3×3 pixel window centered on (x_0, y_0) when we regard them as static points. However, in the actual situation, the intensity of the star will decrease and the shape of the star will change from point-like to short streak-like forms due to the influence of platform vibration and tracking error on the long exposure time. Fig. 9 illustrates the 2-D case as an example.

The streak-like Airy disk model is defined as follows:

$$I(\Phi, t) = \begin{cases} I_0, & \Phi = 0 \\ \dfrac{1}{t_e} \int_0^{t_e} I_0 \left[\dfrac{2J_1(\Phi)}{\Phi} \right]^2 dt, & \Phi \neq 0 \end{cases} \tag{21}$$

$$\Phi = ((x - (x_0 + v_x t))^2 + (y - (y_0 + v_y t)^2)^{1/2} \tag{22}$$

where t_e is the exposure time, (x_0, y_0) is the central coordinates of the stars in the initial position, and v_x and v_y are the image motion speed in the horizontal and vertical directions, respectively.

The Fig. 10 shows the 3-D grayscale histogram of the streak-like target.

TABLE 1. SNRs of typical background stars in the image.

Exposure time	Magnitude of background stars	SNR
3 s	9.5	30
	13.0	3
	13.5	2

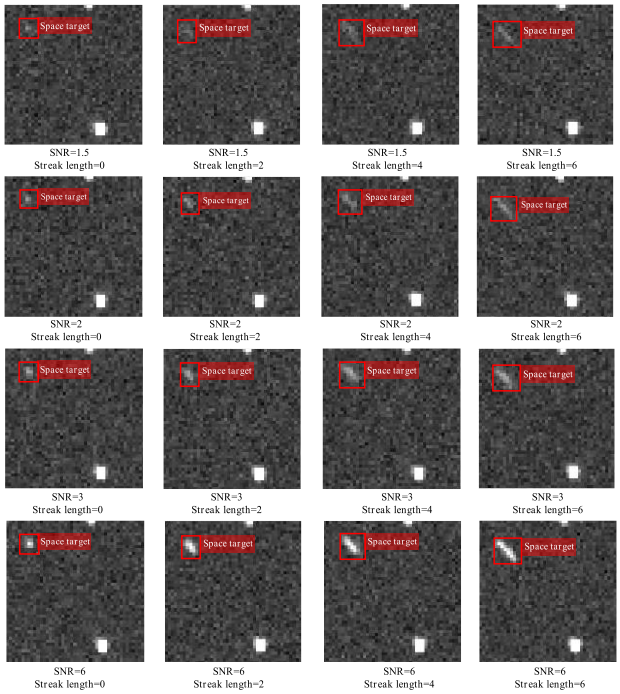

FIGURE 11. Simulated space targets with different streak lengths and SNR.

Before simulating stars and space targets with different SNRs. SNR is defined as follows:

$$SNR_i = \frac{S_e}{\sqrt{S_e + \sigma_R^2 + N_d + N_s}} \tag{23}$$

$$SNR = \frac{\sum_{i=1}^{N_0} SNR_i}{N_0} \tag{24}$$

where SNR_i represents the signal-to-noise ratio of a single pixel in the image, S_e is the number of signal electrons in the target pixel; and σ_R, N_d, and N_s refer to the detector readout, dark current, and stray light noises, respectively.

In Eq. (22), SNR represents the signal-to-noise ratio of the target, N_0 represents the number of pixels in the target's 80% energy region. For example, N_0 will be set to $N_0 = 9$ if 80% energy exists in the 3×3 pixel region of the target.

According to the Tycho-2 catalogue and the optical system, the position and intensity values of background stars are simulated. Table 1 lists the signal-to-noise ratios of typical background stars in the image.

The Fig. 11 shows that the simulated space targets with different streak lengths and SNRs are added to the background image of the stars.

B. DETECTION EXPERIMENTS ON THE SIMULATED IMAGES

Space targets are added to the simulated background star images. We can determine the number, position, SNRs, and streak length of space targets freely.

We performed a series of experiments using the test datasets simulated according to the Tycho-2 Catalogue. The datasets contains four groups and each group has 500 simulated images, including a total of 1200 space targets. The SNRs of these space targets in each group are 6, 3, 2 and 1.5 with streak lengths range from 4 to 10, as shown in Fig. 12.

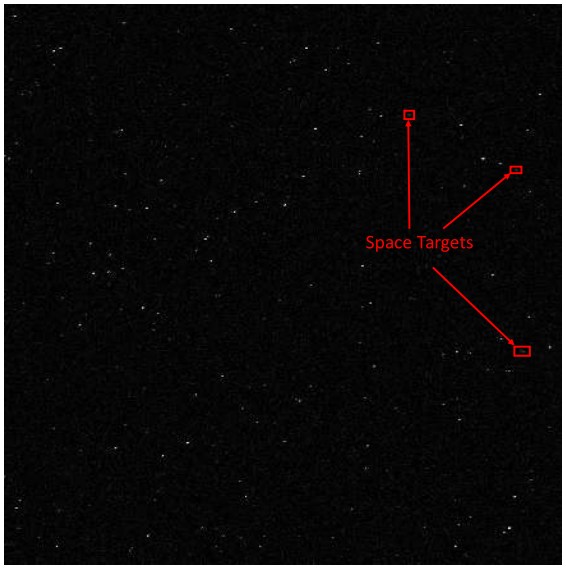

FIGURE 12. Simulation image. (Three simulated space targets exist with SNR 3 in this 1024 × 1024 image).

The proposed spatiotemporal pipeline filtering method was first performed to remove the background stars and noise and obtain candidate points in single frame image. Compared with the time-index filtering method [31], max-mean method [33] and top-hat method [34], the proposed spatiotemporal pipeline filtering method can remove the stars and noise to a large extent.

The receiver operating characteristic (ROC) curves for the four groups of simulated images with different SNRs are shown in Fig. 13.

As shown in Fig. 13, the ROC curves for different SNRs show that, although the detection probabilities become lower as the SNR becomes lower, our method always achieved the best AUC performance: 82.12%, 88.25%, 96.50% and 98.91% for the four categories of SNR=1.5, SNR=2, SNR=3, and SNR=6, respectively.

The detection probability can be improved further when the multistage hypothesis testing stage is performed because the discontinuous and nonlinear trajectories can also be detected, and the false alarms caused by isolated noise points cannot pass the hypotheses test.

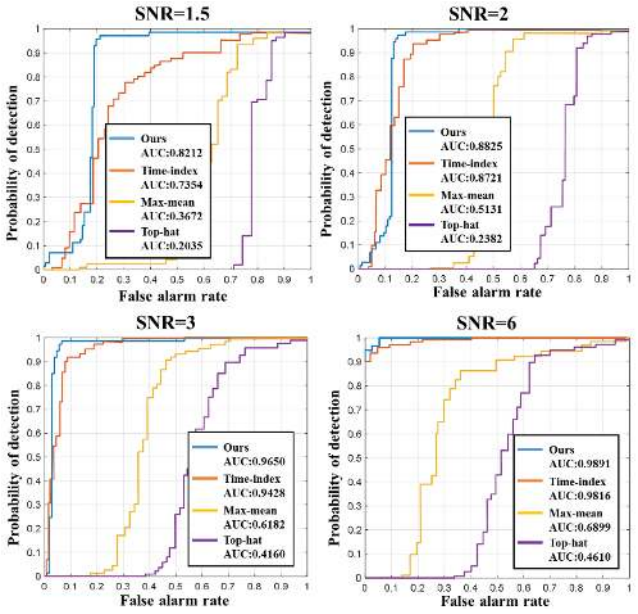

FIGURE 13. Simulation image. (Three simulated space targets exist with SNR 3 in this 1024 × 1024 image).

TABLE 2. Statistical results of space target detection.

SNR	Detection Probability (%)			False Alarm Rate (%)		
	MHT	TMQHT	SPMHT	MHT	TMQHT	SPMHT
6	97.5	98.7	100	2.1	0	0
3	95.0	98.5	**100**	3.4	0	0
2	86.7	96.2	**99.2**	7.0	1.7	**1.3**
1.5	75.0	90.4	**92.7**	18.0	5.8	6.7

Thus, the spatiotemporal pipeline filtering method can perform background stars and noise removal with a loose threshold ($t_s = 0.6$) and obtain a higher detection probability than other methods with the same false-alarm rate.

Then, the detection probability and false alarm rate of SPMHT are evaluated in the test datasets. Table 2 present the test results.

To prove the advantages of the proposed algorithm, Table 2 shows that MHT and TMQHT are used to detect the same targets in datasets. Our SPMHT method can detect all the space targets successfully as long as the SNR of the space target is greater than 3. When SNR is equal to 2, the detection probability is 99.2% with low false alarm rate. Even when SNR is as low as 1.5, the detection probability of the proposed method can still reach 92.7% with 6.7% false alarm. Table 2 presents that the SPMHT method obtains higher detection probability than the other methods in the SNR range of 6 to 1.5. The SPMHT method obtains better performance in detect space targets with low SNR and different orbital velocities (streak lengths range from 4 to 10) than the other methods.

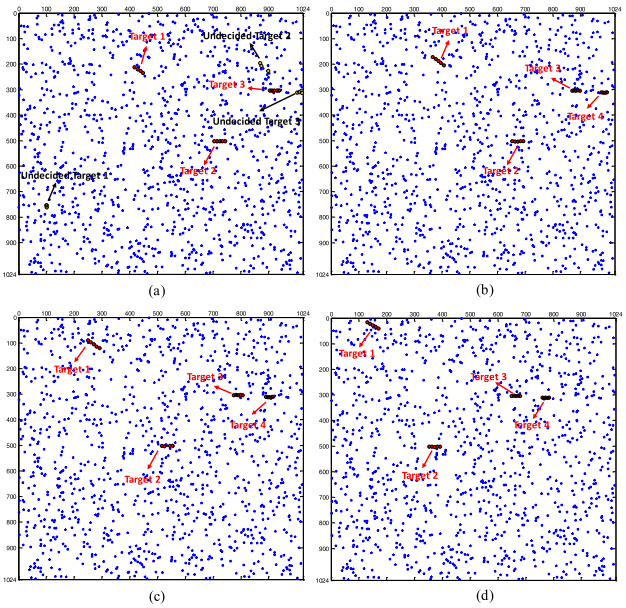

FIGURE 14. Space target detection results of the frame sets (a) 2 (frames 6–10), (b) 3 (frames 11–15), (c) 5 (frames 21–25), and (d) 7 (frames 31–35).

Our algorithm was further analyzed to evaluate its performance in terms of detection and false alarm rejection of discontinuous trajectories. Four simulated space targets have an SNR of 3 in the frame sets. Fig. 14 presents the detection results. The red and yellow circles in the image are the centroids of the detected real space targets and the trajectory points of the undecided space targets, respectively. The detected stars are denoted by the blue pentagrams.

The results show that four simulated space targets are detected successfully. In frame sets 2 and 3, three undecided space targets show up (in frames 6–10 in frame set 2). Both undecided pieces of space debris have only three trajectory points. In frame set 2, the three undecided pieces of targets are checked. Undecided targets 1 and 2 have no succeeding trajectory points, thereby confirming that these are false alarms and removed in the subsequent frame set 3. By contrast, undecided target 3 has 5 continuous trajectory points (8 points in total from frame sets 2 and 3), thereby confirming that this undecided target is an actual piece of space target. In frame set 5 (frames 21–25), Fig. 15 shows that we failed to detect the trajectory point of target 2 in frame 23 because the position of space target 2 overlaps with stars in the current image frame, which is a single frame (frame 23). Target 2 is detected successfully although it has 4 discontinuous trajectory points. Our proposed detection method uses five frames to determine the target, and can detect effectively when up to two targets are lost in a single trajectory.

We further analyze nonlinear and crossed situations of the space target trajectories. The SNR of the space target is also set to 3. Fig. 16 shows the detection results.

The experiment shows that the proposed algorithm detects not only space targets with different orbital velocities and directions of motion but also checks the undecided targets, deletes false alarms, and detects new space targets coming into the field of view in time. When points of space targets in the trajectories are missing because of the covering of background stars or the interference of random background noise, trajectories can still be detected successfully. Even when target trajectories are nonlinear or crossed in image sequences, the proposed SPMHT method can still obtain good performance.

C. DETECTION EXPERIMENTS ON REAL IMAGES

Real sequential image datasets used in the experiments were captured by using the CMOS telescope, which has $10\text{K} \times 10\text{K}$ imaging pixels, 12 bits of grayscale, $10° \times 10°$ field of view, and exposure time of 3s. The optics we used can collect 80% of intensities of space targets and stars in a 3×3 window. These images are captured on the ground in the sidereal tracking mode, in which the telescope is mounted on a turntable with a velocity to counteract that of the Earth's rotation. Both space target and background star images appear as streak-like sources, and these background star images are affected by the platform vibration and tracking error in long exposure times. The Fig. 17 presents part of the images that contains multiple space targets.

The SPMHT method was tested on the real image datasets (600 images) captured by the telescope with 3s exposure time at different times.

To verify the advantages of the proposed method, MHT [28], TMQHT [31] and stacking method [22] are used to detect the same four image sequences. Table 3 lists the detection results.

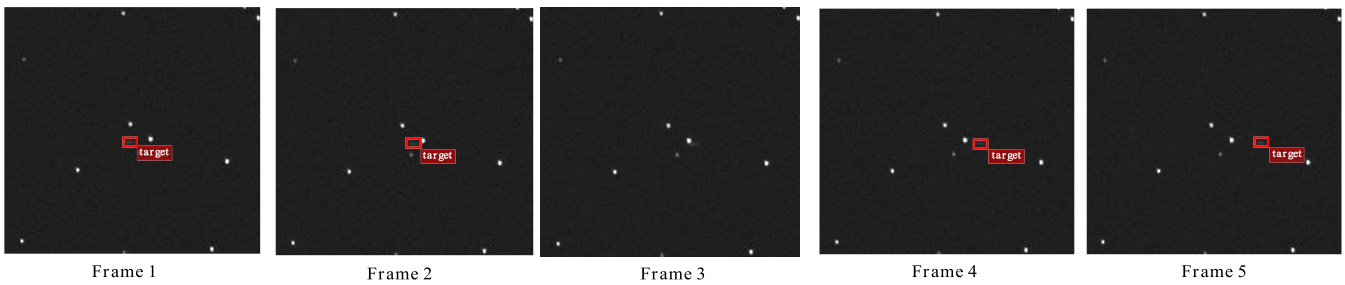

FIGURE 15. Discontinuous trajectory (target 2 in frame set 5).

TABLE 3. Statistical results of space target detection.

Method	GT	Detection Probability	False Alarm Rate	Time	Programming Language
MHT	2892	87.5%	15.2%	28.04s	C++ & Matlab
TMQHT	2892	90.8%	5.2%	2.35s	C++ & Matlab
Stacking Method	2892	93%	68.2%	0.12s	Matlab
ours	2892	98.2%	6.1%	0.68s	C++ & Matlab

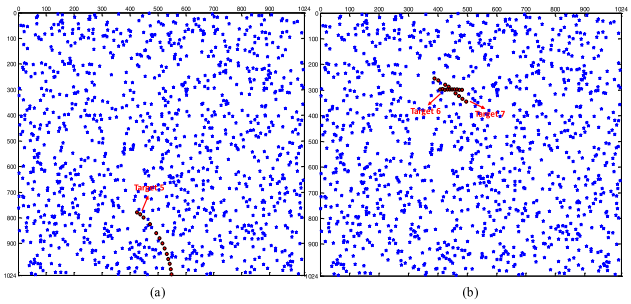

FIGURE 16. (a) Space target detection results of the nonlinear trajectory by using SPMHT with 15 frames, (b) Space target detection results of the crossed trajectory by using SPMHT with 10 frames.

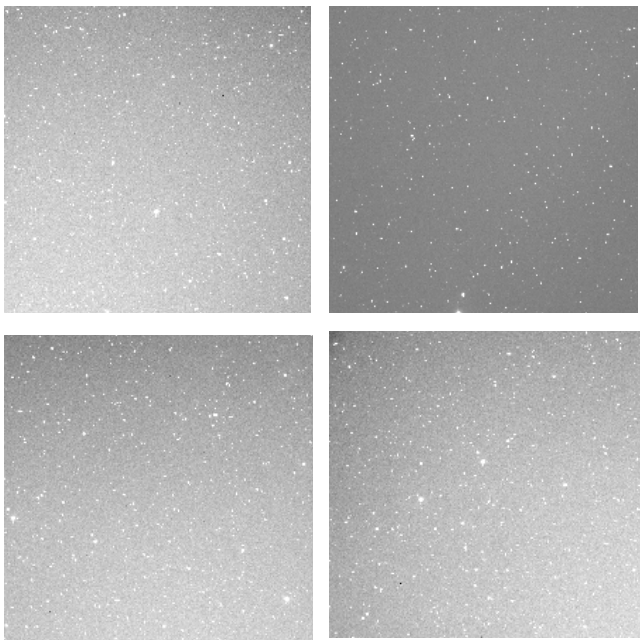

FIGURE 17. Images captured by the space surveillance telescope.

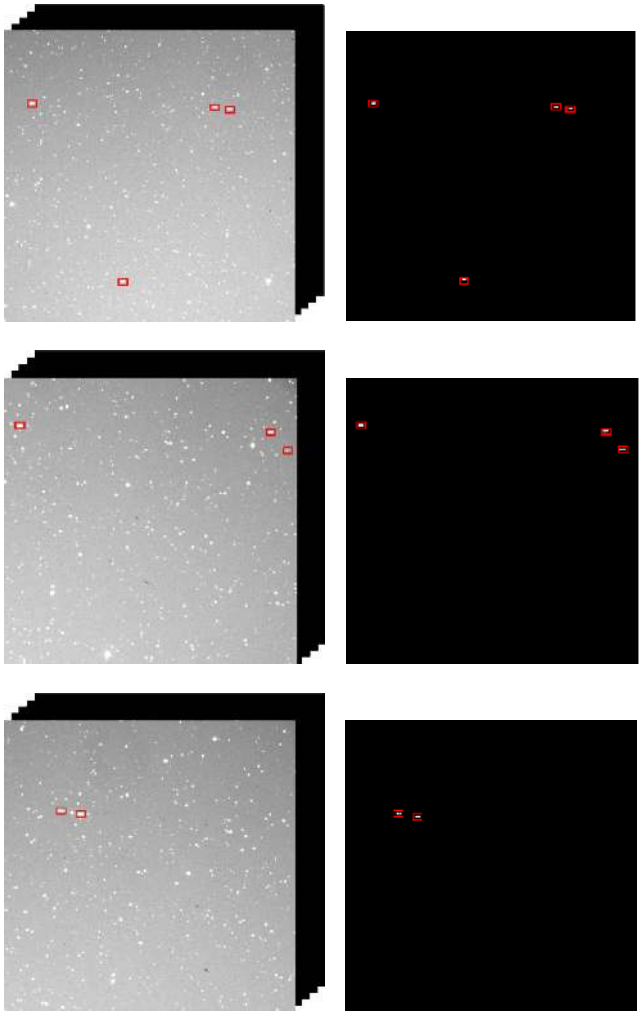

FIGURE 18. Visualization of the detection results of proposed SPMHT in real image datasets.

In the MHT method, detection is performed at every pixel in every image of the sequence, and the candidate trajectories increase rapidly as the number of test stages increases, which cause the large computational cost. TMQHT method overcomes the defects of large computational cost by using the time-index filtering and bright star intensity enhancement. In the hypothesis testing stages, TMQHT method pruned in the tree structure combined with these candidate trajectories by using prior information of moving objects. However, the prior information is a fixed value, which cause the failure to detect targets with different orbital velocities. The detection result of the stacking method is affected by the rotated streak image of background stars in long exposure times and wide-field surveillance. This method obtains very high false alarm rates and has extremely poor robustness.

The SPMHT method overcomes the defects of the above method, which cannot detect space targets well in

complicated situations and has a large computational cost. The results indicate that the proposed SPMHT method has high detection probability and strong robustness. Part of the detection results are shown in Fig. 18.

V. CONCLUSION

In this study, we present a method for detecting space targets in complicated situations for wide-field surveillance. In the case of long exposure time and wide field of view, background stars are affected by platform vibration and tracking error and usually manifest a streak-like form, which are similar to the shape of space targets. The proposed spatiotemporal pipeline with a diameter of 5 pixels can effectively eliminate the similarity interference of streak-like background stars in space target detection. Compared with the traditional classification method based on gray value correlation, SrIoU score has the better detection performance for low SNR targets. After removal of background stars, a tree structure combined with a set of candidate points is established and then pruned at every point in every image of the sequence via hypothesis testing. The adaptive distance d and cosine θ thresholds in hypothesis testing conditions can solve the difficulties in detecting space targets with different orbital velocities and nonlinear trajectories. The simulation and experimental results show that the proposed SPMHT method clearly outperforms the state-of-the-art target detectors. Moreover, the proposed method demonstrates good robustness and low computational cost to overcome the difficulties for space targets detection in complicated situations for wide-field surveillance.

In our future work, we plan to improve our method and apply it not only in the presence of noise and vibration, but also in the presence of stray light. We also intend to implement our method in a real-time system for space-based wide-field surveillance.

REFERENCES

[1] H. Wirnsberger, O. Baur, and G. Kirchner, "Space debris orbit prediction errors using bi-static laser observations. Case study: ENVISAT," *Adv. Space Res.*, vol. 55, pp. 2607–2615, Jun. 2015.

[2] B. Esmiller, C. Jacquelard, H.-A. Eckel, and E. Wnuk, "Space debris removal by ground-based lasers: Main conclusions of the European project CLEANSPACE," *Appl. Opt.*, vol. 53, no. 31, pp. 145–154, 2014.

[3] J. Núñez, A. Núñez, F. J. Montojo, and M. Condominas, "Improving space debris detection in GEO ring using image deconvolution," *Adv. Space Res.*, vol. 56, no. 2, pp. 218–228, 2015.

[4] T. Ye and F. Zhou, "Autonomous space target recognition and tracking approach using star sensors based on a Kalman filter," *Appl. Opt.*, vol. 54, no. 11, pp. 3455–3469, 2015.

[5] B. Sease, B. Flewelling, and J. Black, "Automatic streak endpoint localization from the cornerness metric," *Acta Astronautica.*, vol. 134, pp. 345–354, May 2017.

[6] R.-Y. Sun, J.-W. Zhan, C.-X. Zhao, and X.-X. Zhang, "Algorithms and applications for detecting faint space debris in GEO," *Acta Astronautica*, vol. 110, pp. 9–17, May/Jun. 2015.

[7] E. Rublee, V. Rabaud, K. Konolige, and G. R. Bradski, "ORB: An efficient alternative to SIFT or SURF," in *Proc. IEEE Int. Conf. Comput. Vis. (ICCV)*, Nov. 2011, pp. 2564–2571.

[8] Z. Guo and D. Zhang, "A completed modeling of local binary pattern operator for texture classification," *IEEE Trans. Image Process.*, vol. 19, no. 6, pp. 1657–1663, Jan. 2010.

[9] N. Dalal and B. Triggs, "Histograms of oriented gradients for human detection," in *Proc. IEEE Comput. Soc. Conf. Comput. Vis. Pattern Recognit.*, Jun. 2005, pp. 886–893.

[10] Y. Sun, J. Yang, Y. Long, Z. Shang, and W. An, "Infrared patch-tensor model with weighted tensor nuclear norm for small target detection in a single frame," *IEEE Access*, vol. 6, pp. 76140–76152, 2018.

[11] J. Gao, Z. Lin, and W. An, "Infrared small target detection using a temporal variance and spatial patch contrast filter," *IEEE Access*, vol. 7, pp. 32217–32226, 2019.

[12] Y. Chen, B. Song, X. Du, and M. Guizani, "Infrared small target detection through multiple feature analysis based on visual saliency," *IEEE Access*, vol. 7, pp. 38996–39004, 2019.

[13] S. C. Loke, "Astronomical image acquisition using an improved track and accumulate method," *IEEE Access*, vol. 5, pp. 9691–9698, 2017.

[14] M.-S. Wei, F. Xing, and Z. You, "A real-time detection and positioning method for small and weak targets using a 1D morphology-based approach in 2D images," *Light Sci. Appl.*, vol. 7, May 2018, Art. no. 18006.

[15] R. Šra, M. Matoušek, and V. Franc, "RANSACing optical image sequences for GEO and near-GEO objects," in *Proc. Adv. Maui Opt. Space Surveill. Technol. Conf.*, 2013, pp. 1–10.

[16] T. Hardy, S. Cain, J. Jeon, and T. Blake, "Improving space domain awareness through unequal-cost multiple hypothesis testing in the space surveillance telescope," *Appl. Opt.*, vol. 54, no. 17, pp. 5481–5494, 2015.

[17] T. Hardy, S. Cain, and T. Blake, "Unequal a priori probability multiple hypothesis testing in space domain awareness with the space surveillance telescope," *Appl. Opt.*, vol. 55, no. 15, pp. 4036–4046, 2016.

[18] M. Tagawa, T. Yanagisawa, H. Kurosaki, H. Oda, and T. Hanada, "Orbital objects detection algorithm using faint streaks," *Adv. Space Res.*, vol. 57, pp. 929–937, Feb. 2016.

[19] J. Virtanen, J. Poikonen, T. Säntti, T. Komulainen, J. Torppa, M. Granvik, K. Muinonen, H. Pentikäinen, J. Martikainen, J. Näränen, J. Lehti, and T. Flohrer, "Streak detection and analysis pipeline for space-debris optical images," *Adv. Space Res.*, vol. 57, pp. 1607–1623, Apr. 2016.

[20] M. Piccardi, "Background subtraction techniques: A review," in *Proc. IEEE Int. Conf. Syst., Man Cybern.*, Oct. 2004, pp. 3099–3104.

[21] I. S. Reed, R. M. Gagliardi, and H. M. Shao, "Application of three-dimensional filtering to moving target detection," *IEEE Trans. Aerosp. Electron. Syst.*, vol. AES-19, no. 6, pp. 898–905, Nov. 1983.

[22] T. Yanagisawa, A. Nakajima, T. Kimura, T. Isobe, H. Futami, and M. Suzuki, "Detection of small GEO debris by use of the stacking method," *Trans. Jpn. Soc. Aero. Space Sci.*, vol. 44, no. 146, pp. 190–199, 2002.

[23] N. C. Mohanty, "Computer tracking of moving point targets in space," *IEEE Trans. Pattern Anal. Machine Intell.*, vol. PAMI-3, no. 5, pp. 606–611, Sep. 1981.

[24] Y. Barniv, "Dynamic programming solution for detecting dim moving targets," *IEEE Trans. Aerosp. Electron. Syst.*, vol. AES-21, no. 1, pp. 144–156, Jan. 1985.

[25] A. E. Cowart, W. E. Snyder, and W. H. Ruedger, "The detection of unresolved targets using the Hough transform," *Comput. Vis., Graph, Image Processing.*, vol. 21, no. 2, pp. 222–238, 1983.

[26] K. Fujita, T. Hanada, Y. Kitazawa, and A. Kawabe, "A debris image tracking using optical flow algorithm," *Adv. Space Res.*, vol. 49, no. 5, pp. 1007–1018, 2012.

[27] K. Fujita, N. Ichimura, and T. Hanada, "Detecting GEO debris via cascading numerical evaluation for lines in image sequence," in *Proc. Adv. Maui Opt. Space Surveill. Technol. Conf.*, 2014, pp. 1–7.

[28] S. D. Blostein and T. S. Huang, "Detecting small, moving objects in image sequences using sequential hypothesis testing," *IEEE Trans. Signal Process.*, vol. 39, no. 7, pp. 1611–1629, Jul. 1991.

[29] G. C. Demos, "Applications of MHT to dim moving targets," *Proc. SPIE*, vol. 1305, pp. 297–309, Oct. 1990.

[30] S. D. Blostein and H. S. Richardson, "A sequential detection approach to target tracking," *IEEE Trans. Aerosp. Electron. Syst.*, vol. 30, no. 1, pp. 197–212, Jan. 1994.

[31] J. Xi, D. Wen, O. K. Ersoy, H. Yi, D. Yao, Z. Song, and S. Xi, "Space debris detection in optical image sequences," *Appl. Opt.*, vol. 55, no. 28, pp. 7929–7940, 2016.

[32] G. Rufino and D. Accardo, "Enhancement of the centroiding algorithm for star tracker measure refinement," *Acta Astronautica*, vol. 53, pp. 135–147, Jul. 2003.

[33] S. D. Deshpande, M. H. Er, V. Ronda, and P. Chan, "Max-mean and max-median filters for detection of small-targets," *Proc. SPIE*, vol. 3809, pp. 74–83, Oct. 1999.

[34] X. Bai and F. Zhou, "Analysis of new top-hat transformation and the application for infrared dim small target detection," *Pattern Recognit.*, vol. 43, no. 6, pp. 2145–2156, 2010.
[35] B. Du, Y. Zhang, L. Zhang, and D. Tao, "Beyond the sparsity-based target detector: A hybrid sparsity and statistics-based detector for hyperspectral images," *IEEE Trans. Image Process.*, vol. 25, no. 11, pp. 5345–5357, Nov. 2016.

MENGYANG LI was born in Heihe, Heilongjiang, China, in 1992. He received the B.S. degree in physics from Jilin University, Changchun, China, in 2015. He is currently pursuing the Ph.D. degree with the Changchun Institute of Optics, Fine Mechanics and Physics, Chinese Academy of Sciences, Changchun, China.

His research interests include image processing, weak target detection, and computer vision.

CHANGXIANG YAN was born in Honghu, Hubei, China, in 1973. He received the M.S. degree in engineering from Zhejiang University, Zhejiang, China, in 1998, and the Ph.D. degree from the Changchun Institute of Optics, Fine Mechanics and Physics, Chinese Academy of Sciences, Changchun, China, in 2001.

Since 2010, he has been the Director of the Space Optics Laboratory, Changchun Institute of Optics, Fine Mechanics and Physics, Chinese Academy of Sciences. His research interests include opto-mechatronics technology for space optical remote sensing instruments, multispectral and hyperspectral spatial remote sensing imaging, polarization detection, and space surveillance.

CHUNHUI HU was born in Xinyang, Henan, China, in 1986. He received the B.S. degree in optical information science and technology from Northwestern Polytechnical University, China, in 2008, and the Ph.D. degree in optical engineering from the Changchun Institute of Optics, Fine Mechanics and Physics, Chinese Academy of Sciences, Changchun, China, in 2013, where, he is currently an Assistant Researcher.

His current research interests include installation and inspection of optical systems.

CHONGYANG LIU was born in Changchun, Jilin, China, in 1992. He received the B.S. degree in space science from Shandong University, Weihai, China, in 2015. He is currently pursuing the Ph.D. degree with the Changchun Institute of Optics, Fine Mechanics and Physics, Chinese Academy of Sciences, Changchun, China.

His research interests include image processing, remote sensing, and computer vision.

LIZHI XU was born in Suizhou, Hubei, China, in 1993. He received the B.S. degree in physics from the University of Science and Technology of China, Hefei, China, in 2015. He is currently pursuing the Ph.D. degree with the Changchun Institute of Optics, Fine Mechanics and Physics, Chinese Academy of Sciences, Changchun, China.

His research interest includes remote sensing.